Plasmonics (2025) 20:11319–11330
https://doi.org/10.1007/s11468-025-03194-y

RESEARCH

Enhanced Surface Plasmon Resonance Detection of Ascorbic Acid Using Carbon Quantum Dots Thin Film

Wan Mohd Ebtisyam Mustaqim Mohd Daniyal[1] · Yap Wing Fen[2,3] · Muhamad Zamri Kariming[3] · Nurul Illya Muhamad Fauzi[2] · Hazwani Suhaila Hashim[3] · Muhammad Fahmi Anuar[2] · Ferry Anggoro Ardy Nugroho[4,5] · Nurul Hidayat[6] · Huda Abdullah[7] · Ahmad Taufiq[6] · Faten Bashar Kamal Eddin[8]

Received: 26 May 2025 / Accepted: 10 July 2025 / Published online: 23 July 2025

Abstract

This research investigates the structural and optical properties of carbon quantum dots (CQDs) for the sensitive detection of ascorbic acid (AA), an essential biomolecule used widely in health and industry. Accurate AA detection is critical for pharmaceutical and food safety applications, and this study demonstrates the use of a prism-based surface plasmon resonance (SPR) sensor with a CQD thin film for label-free and real-time monitoring. CQDs were deposited onto a gold (Au) thin film, and their structural properties were characterized through Fourier transform infrared spectroscopy (FTIR) and atomic force microscopy (AFM). FTIR analysis confirmed the presence of C–H, C≡C, C–N, and C–O bonds on the Au/CQDs surface, while AFM characterization revealed that the CQDs formed a uniformly dispersed, spiky surface evenly distributed across the gold layer. The optical properties of the Au/CQDs thin film were studied using ultraviolet–visible (UV–Vis) spectroscopy, showing an absorption peak of approximately 4.44 a.u. in the range of 260–270 nm, with an optical bandgap of 4.072 eV. When integrated into the SPR sensor, the Au/CQDs thin film demonstrated high sensitivity for AA detection, achieving a detection limit as low as 0.001 μM. Further characterization was conducted to explore the interaction between the Au/CQD thin film and AA, highlighting the film's potential for use in sensitive biochemical sensing applications.

Keywords Surface plasmon resonance · Carbon quantum dots · Ascorbic acid · Optical sensor

Introduction

Ascorbic acid (AA), commonly known as vitamin C, has the molecular formula of $C_6H_8O_6$, plays a vital role in human health due to its antioxidant properties, which are crucial for preventing oxidative stress and supporting the immune system [1, 2]. AA is also essential for biosynthesis of collagen, carnitine, and neurotransmitters in the human body [3, 4]. Additionally, AA is widely used in the food and pharmaceutical industries as an additive and preservative, making its accurate detection important for quality control and regulatory compliance [5, 6]. According to the European Food Safety Authority, the recommended average daily intake of AA (vitamin C) for adults is approximately 90 mg [7].

✉ Yap Wing Fen
yapwingfen@upm.edu.my

1 Physics Section, School of Distance Education, Universiti Sains Malaysia (USM), George Town, Pulau Pinang 11800, Malaysia

2 Functional Nanotechnology Devices Laboratory, Institute of Nanoscience and Nanotechnology, Universiti Putra Malaysia (UPM), Serdang, Selangor 43400, Malaysia

3 Department of Physics, Faculty of Science, Universiti Putra Malaysia (UPM), Serdang, Selangor 43400, Malaysia

4 Department of Physics, Faculty of Mathematics and Natural Sciences, Universitas Indonesia, Depok 16424, Indonesia

5 Institute for Advanced Sustainable Materials Research and Technology, Faculty of Mathematics and Natural Sciences, Universitas Indonesia, Depok 16424, Indonesia

6 Department of Physics, Faculty of Mathematics and Natural Sciences, Universitas Negeri Malang, Jl. Semarang 5, Malang 65145, Indonesia

7 Department of Electrical, Electronic and System Engineering, Faculty of Engineering and Built Environment, Universiti Kebangsaan Malaysia, Bangi 43600, Malaysia

8 Centre for Optical and Electromagnetic Research, College of Optical Science and Engineering, Zhejiang University, Hangzhou 310058, China

High levels of AA intake can cause various health problems that includes undesired gastrointestinal and renal effects while deficiency of AA can affect protein metabolism, iron absorption, and immune system [8–10]. Therefore, the ability to detect ascorbic AA at low concentrations is important. Traditional methods of AA detection, such as titration and chromatography, while effective, can be time-consuming, require complex sample preparation, and may not be sensitive enough for detecting low concentrations. Given these challenges, there is a growing demand for more efficient, sensitive, and rapid detection methods.

To meet this demand, a variety of biosensing technologies have been developed, including optical, electrochemical, thermometric, piezoelectric, and magnetic methods. Among these, surface plasmon resonance (SPR) spectroscopy is the most popular and widely accepted by researchers due to its advantages in chemistry, biological sciences, and other fields [11–18]. Since it was applied for gas detection and biosensing in 1982, the SPR sensor has been well known in the scientific community. SPR works based on a fundamental principle of physics involving light behavior at the boundary of materials with different refractive indices. When light travels from a medium with a higher refractive index, such as glass, into one with a lower refractive index, like air, total internal reflection occurs if the angle of incidence exceeds the critical angle. If a thin metal layer such as typically gold is placed at the interface between the glass and air, the energy from the reflected light can couple with surface plasmons on the metal [19–21]. This coupling causes a reduction in the intensity of the reflected light, producing a resonance at a specific angle, known as resonance angle [22–29]. SPR works by measuring the changes of the refractive index value near the surface of metal layer. The changes of refractive index will also change the resonance angle, making SPR suitable as a sensor [30–39]. Compared to other sensors, SPR stands out due to its numerous advantages, including linear response, cost-effectiveness, rapid and real-time measurements, non-invasive nature, small sample requirements, label-free detection, and high sensitivity [40–42]. These benefits make SPR an attractive choice for a wide range of applications across various fields and highly favored by researchers. Moreover, recent advances in nanotechnology have enabled the integration of novel materials with SPR platforms, further enhancing sensor performance and paving the way for next-generation detection systems.

Carbon-based nanomaterials, such as carbon nanoparticles and carbon nanotubes, are among the most well-known and extensively studied nanomaterials due to their remarkable capabilities which involve magnetic and optical characteristics, including ease of access, environmentally friendly, high stability, and outstanding catalytic properties [43–46]. Carbon quantum dots (CQDs) are also one of the carbon-nanomaterials which have attracted tremendous interest of researchers because of their exceptional features that include low toxicity, excellent stability, excellent biocompatibility, and excellent light absorption properties [47–49]. One of the crucial optical features of CQDs is the photoluminescent properties. CQDs are known for their strong fluorescence stability, allowing them to maintain a steady emission intensity even after extended periods of continuous excitation [50–52]. In addition, their surfaces can be functionalized with specific recognition elements enhancing their sensitivity and selectivity. These distinctive properties make CQDs a compelling choice for sensor applications. Previous research shows that CQDs have been integrated in several sensors to detect various targets, such as cysteine, dopamine, antipsychotics, curcumin [53–60]. To the best of our knowledge, sensing of AA using SPR optical sensor with CQDs as the sensing material has not been reported. Hence, in this present work, CQDs have been integrated into the SPR sensor to improve the

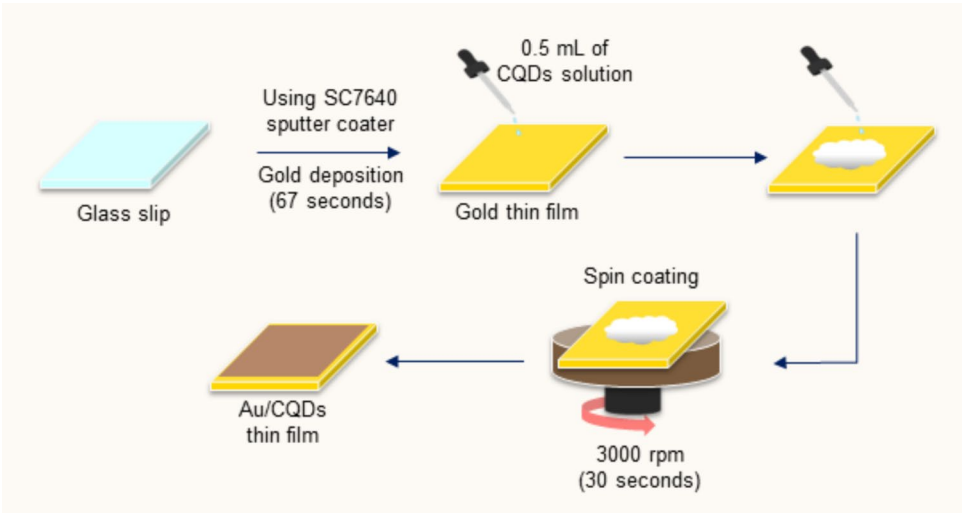

Fig. 1 Preparation of Au/CQDs thin films

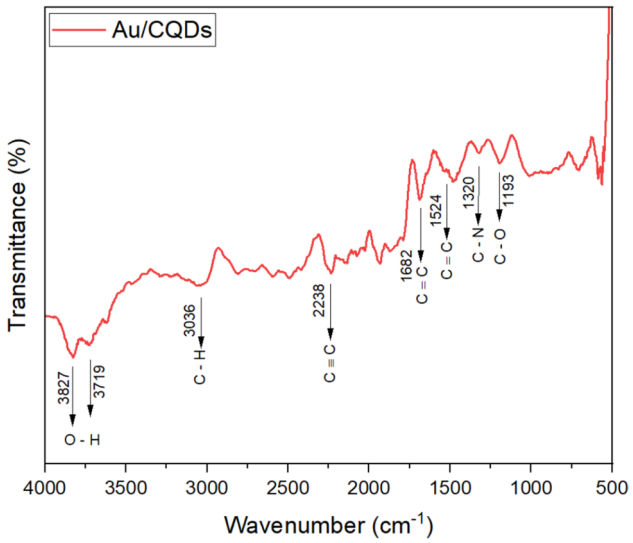

Fig. 2 FTIR spectrum of the Au/CQD thin film where the broad band is near 3827–3719 cm^{-1} (O–H stretching), a prominent peak is around 3036 cm^{-1} for C–H stretching, C≡C stretching at 2238 cm^{-1}, C=C stretching at 1682 cm^{-1} and 1524 cm^{-1}, C–N stretching at 1320 cm^{-1}, and C–O stretching at 1193 $cm.^{-1}$

sensing capabilities for AA detection. Additionally, the structural and optical properties of the CQDs thin film were also characterized to support and validate the sensing behavior.

Materials and Methods

Reagent and Materials

Carbon quantum dots (CQDs) were purchased from the Sabanci University Nanotechnology Research and Application Center (SUNUM) Turkey, and AA was purchased from Sigma-Aldrich. Deionized water (DW) was used throughout the experiments and characterization. A prism with refractive index $n = 1.77861$ and glass coverslip 24 mm × 24 mm × 0.1 mm were purchased from Menzel-Glaser.

Preparation of Au/CQDs Thin Film

The formation of thin film was produced by applying a spin coating method. First, the glass slip was cleaned with acetone to remove any dirt or fingerprint imprints from the glass slips. After that, the glass slips were coated with a thin layer of gold by using SC7640 Sputter Coater. The sputtering time was set to 67 s followed by 5 psi gas pressure and 25-mm distance between the substrate and target to obtain 50-mm gold thickness. Next, approximately 1 mL of the CQD solution was placed on the surface of gold-coated glass slips. Then, the glass slips were spun at 3000 rpm for 30 s using the Specialty Coating System, P-6708D, to produce the Au/CQD thin film. Figure 1 shows the illustration of preparation of the Au/CQDs thin films.

Preparation of Ascorbic Acid Solution

To prepare the AA solution with varying concentrations, 1 g of the AA was diluted using standard dilution principles. The distilled water was used to produce AA solutions with concentrations of 0, 0.001, 0.01, 0.1, 1, 10, 100, 1000, and 10,000 µM.

Instrumental

The Fourier transform infrared (FTIR) spectrum of the sample ranging from 400 to 4000 cm^{-1} was obtained using a Perkin-Elmer spectrophotometer (CA, USA). The surface morphology of the thin films was analyzed using atomic

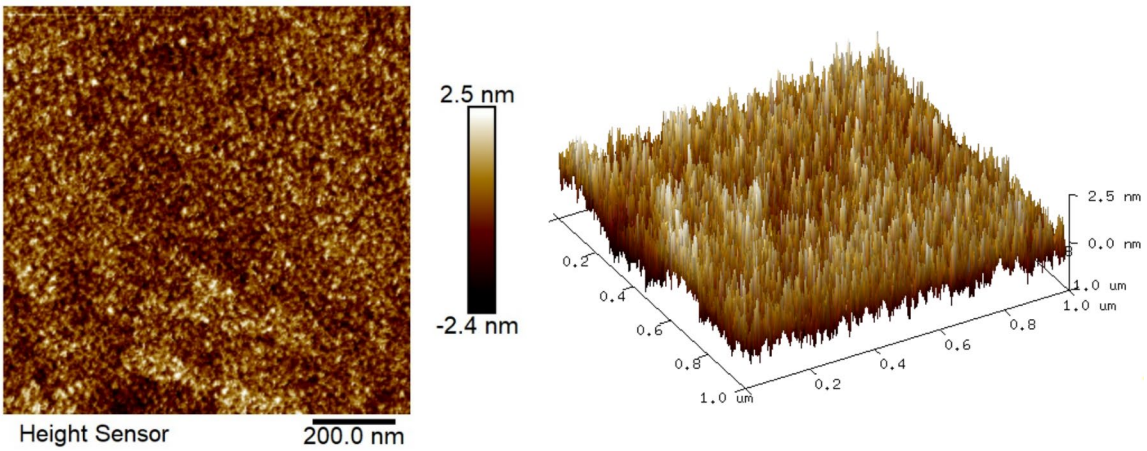

Fig. 3 AFM result of the Au/CQD thin film

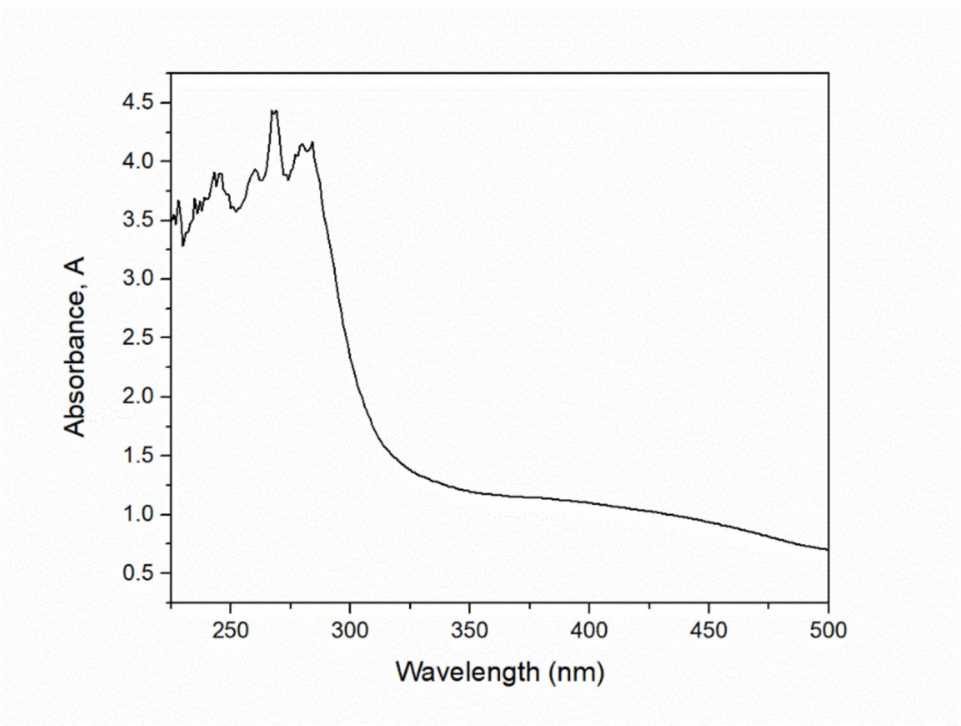

Fig. 4 Absorbance spectrum of the Au/CQD thin film

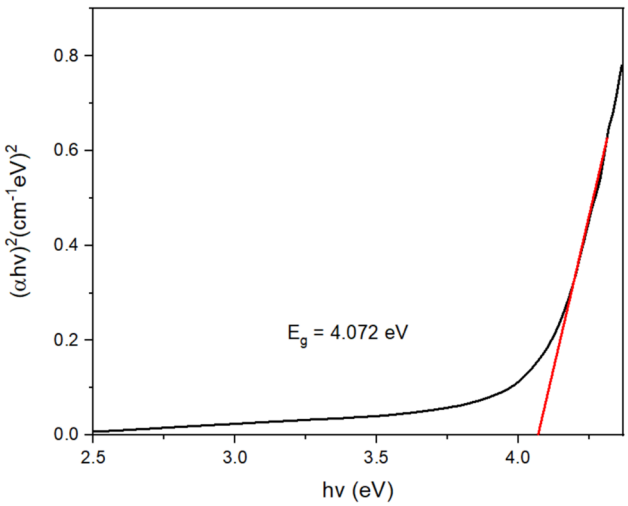

Fig. 5 Optical band gap for the Au/CQD thin film

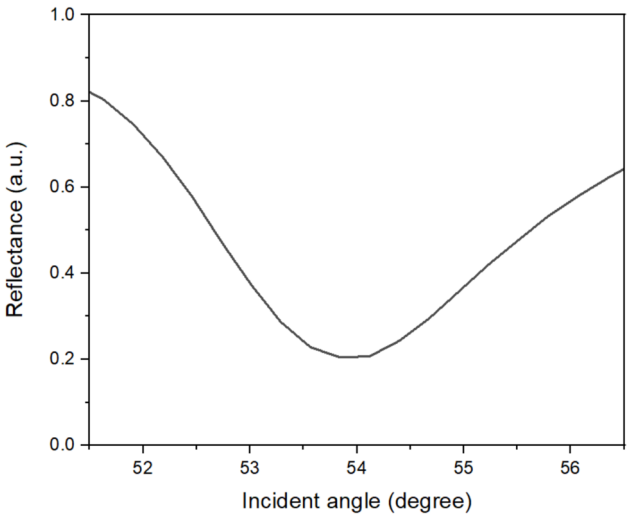

Fig. 6 SPR reflectivity curves of gold layer in-contact with deionized water (DW)

force microscopy (AFM) (Bruker Multimode 8). The UV–vis spectrum was recorded using a UV–vis spectrophotometer (UV-3600, Shimadzu).

Surface Plasmon Resonance (SPR) Technique

In this study, the Kretchmann configuration was applied to evaluate the potential of Au/CQDs thin films to detect the AA in the range of 0 to 10 mM. A He–Ne laser, a polarizer, an optical chopper (SR 540), and an optical stage driven by a stepper motor with a resolution of 0.001° (Newport MM 3000) comprise the SPR setup. The Au/CQDs thin film was sandwiched between the glass prism and hollow. Then, the AA solution will be injected into the hollow before the signal was recorded. This process was repeated using different concentrations of AA. In this configuration, with a 50-nm gold layer and 632.8-nm excitation wavelength, the evanescent plasmon field is estimated to penetrate approximately 200 nm into the sensing medium [61, 62]. This penetration

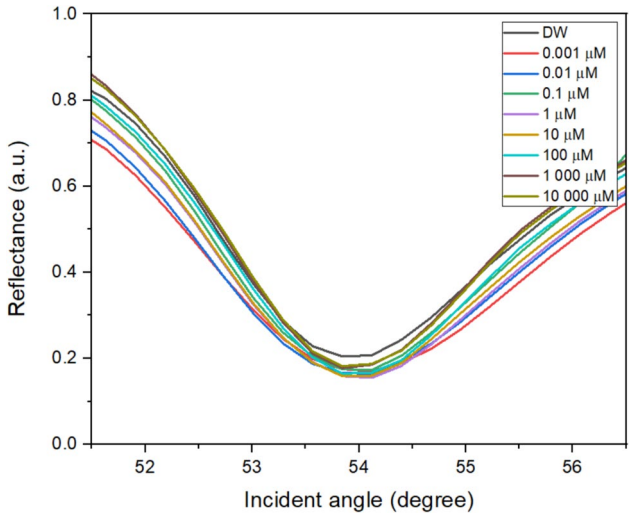

Fig. 7 SPR reflectivity curves of gold layer in-contact with different concentrations of ascorbic acid (AA) 0 to 10,000 µM

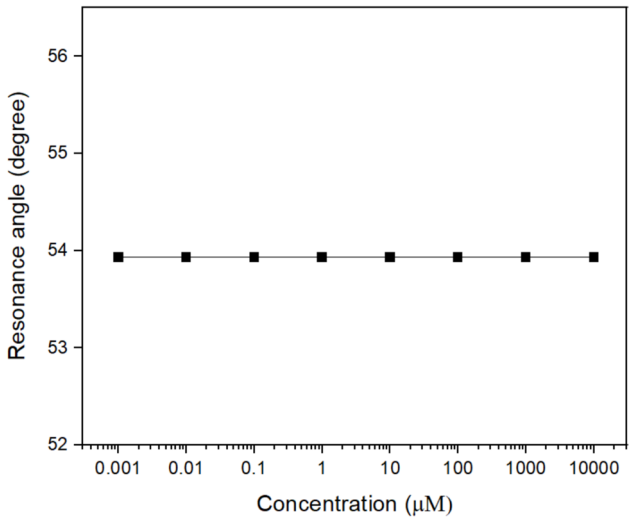

Fig. 8 The resonance angle of gold surface in-contact with different AA concentrations

depth ensures that the interaction between the analyte and the CQDs layer occurs well within the sensitive region of the SPR field and is comparable to those reported in previous SPR-based sensing studies [63–65].

Results and Discussion

FTIR Analysis

An FTIR analysis was conducted to investigate the functional groups present in the Au/CQD thin film within the

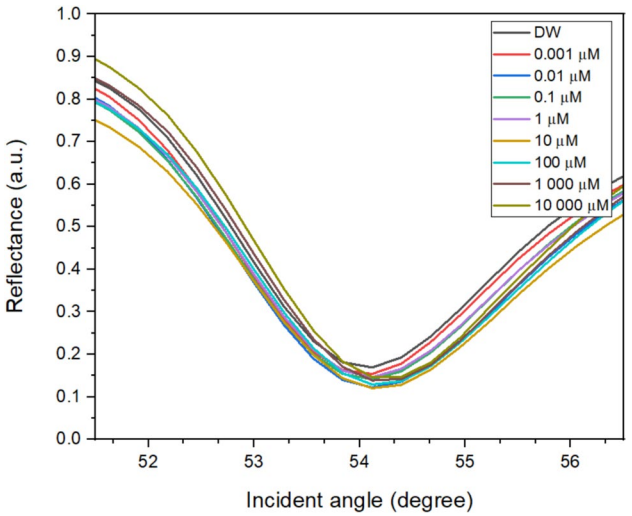

Fig. 9 SPR reflectivity curves for the Au/CQD thin film in-contact with different concentrations of AA that ranged from 0 to 10,000 µM

Table 1 The SPR resonance angle and shift resonance angle for different concentration of AA solution in-contact with the Au/CQD thin film (0 µM represents deionized water)

Concentration of AA (µM)	Resonance angle, θ (degree)	Shift resonance angle, $\Delta\theta$ (degree)
0	54.07	0
0.001	54.08	0.01
0.01	54.13	0.06
0.1	54.14	0.07
1	54.15	0.08
10	54.21	0.14
100	54.23	0.16
1,000	54.25	0.18
10,000	54.26	0.19

infrared spectral range of 4000 to 500 cm^{-1}. The FTIR spectrum revealed prominent absorption peaks, identifying key functional groups in the thin film, as shown in Fig. 2. Peaks at 3827 cm^{-1} and 3719 cm^{-1} associated with the O–H stretching vibrations. This confirmed the presence of hydroxyl groups, consistent with findings by Kamal Eddin et al. [66]. Additionally, a peak at 3036 cm^{-1} indicated C–H stretching vibrations, while the peak at 2238 cm^{-1} corresponded to the alkyne C≡C stretching frequency. Furthermore, the spectrum displayed peaks at 1682 cm^{-1} and 1524 cm^{-1} attributed to C=C stretching vibrations [67]. Peaks at 1320 cm^{-1} and 1193 cm^{-1} were assigned to C–N and C–O stretching bonds, respectively. These peaks have good agreement with prior studies by Liu et al. and He et al., which documented the C–N and C–O stretching ranges between 1266 and 1310 cm^{-1} and between 1163 and 1210 cm^{-1}, respectively [68, 69]. The presence of these

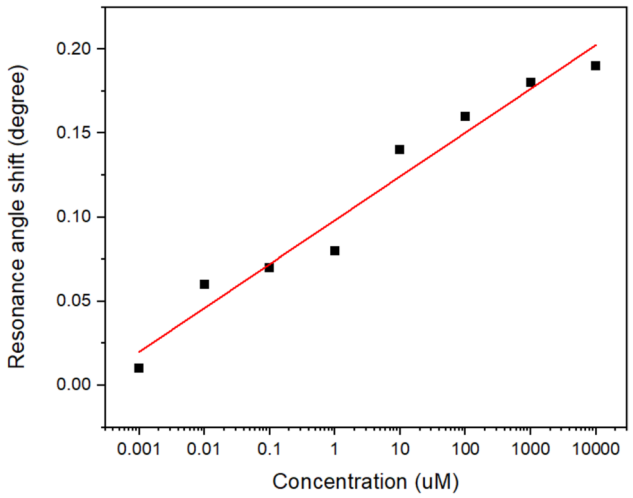

Fig. 10 SPR angle shift against AA concentration for CQD thin film

diverse functional groups indicates that the Au/CQDs thin film possesses a rich surface chemistry capable of aiding in bond formation or interactions with AA. These functional groups are capable of forming hydrogen bonds or electrostatic interactions with AA molecules. Such interactions contribute to the changes in the refractive index at the sensor surface, which are crucial for generating SPR signal shifts.

AFM Analysis

The structural properties of the Au/CQDs thin film were further characterized using atomic force microscopy (AFM) in tapping mode. Figure 3 presents both two-dimensional (2D) and three-dimensional (3D) AFM images of the Au/CQD thin film. The images revealed a uniformly dispersed spiky surface, with CQDs evenly scattered across the gold-coated glass substrate. The root mean square (RMS) roughness measured was 0.736 nm indicating a moderately textured nanoscale surface. This homogeneous sensing layer on the gold thin film is critical for consistent surface interactions while the spiky topography contributes to a larger effective surface area which allows for more efficient interaction with AA molecules. This in turn will enhance the adsorption of ascorbic acid and amplifies changes in the refractive index [70].

UV–Vis Analysis

The optical properties of the Au/CQDs thin film were determined by examining the absorbance spectrum at various wavelengths between 220 and 500 nm. Figure 4 shows the thin film materials' absorbance curves. As shown in the figure, the absorbance peak of the Au/CQD thin film was approximately 4.4 in the range of 260 to 270 nm. The strong absorbance peak of CQDs might due to the π–π* transition of aromatic C = C bond [71]. The absorbance peak of the Au/CQDs thin film is crucial in determining the optical band gap.

In this study, the Beer-Lambert Law was applied to determine absorbance, which is directly proportional to the concentration of the chemical species. The optical band gap E_g for the Au/CQD thin film, calculated as the zero point of the linear fit from a plot of $(\alpha hv)^2$ versus hv, is found to be 4.072 eV. This value aligns well with previous findings by Ramdzan et al. [72]. Figure 5 presents the $(\alpha hv)^2$ against the hv plot for the Au/CQDs thin film.

Surface Plasmon Resonance

SPR test was first conducted with deionized water (DW) in-contact with the gold layer. About 3 ml of DW was inserted

Table 2 Sensing properties of various sensors for AA detection

Method	Materials/substrate	Lowest detection	Detection range	References
Colorimetric	Silver nanoparticles	0.0792 µM	0.25–50.0 µM	[75]
Colorimetric	Maltol capped silver nanoparticles	0.064 µM	0–1 µM	[76]
Fluorescence	Cerium-based nanoparticles	8.0 µM	0.01–40 mM	[77]
Colorimetric		8.4 µM	0.01–50 mM	
Fluorescence	Phosphorus/nitrogen dual doped carbon quantum dot	0.023 µM	1.5 – 30 µM	[78]
Fluorescence	Carbon quantum dots – MnO_2	0.042 µM	0.18 – 90 µM	[79]
Fluorescence	Carbon quantum dots	0.1 µM	5–100 µM	[80]
Fluorescence	Fe^{3+}-functionalized carbon quantum dots	0.0091µM	0.1–50 µM	[81]
Fluorescence	N-doped carbon quantum dots	0.093 µM	0–130 µM	[82]
Fluorescence and LSPR	Au@MnO_2 nanoparticles	0.47 µM 0.18 µM	0.75–17.5 µM	[83]
LSPR	Germanium-doped photosensitive fiber	15.12 µM	40–120 µM	[84]
SPR	Silver nanoparticles	0.08 µM	0.5–60 µM	[85]
SPR	Carbon quantum dots (CQDs)	0.001 µM	0.001–10,000 µM	This work

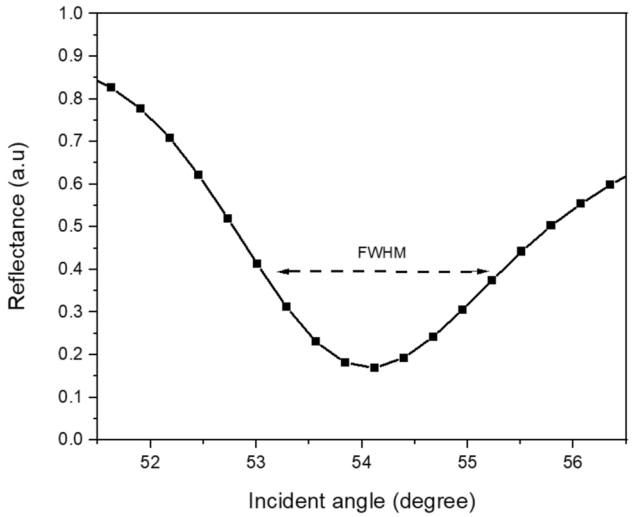

Fig. 11 FWHM of SPR reflectivity curve

Table 3 Values of FWHM and DA of Au/CQDs active layer in-contact with different concentrations of AA

Concentration of AA (μM)	Full width half maximum, FWHM (degree)	Detection accuracy, DA (degree^{-1})
0	2.252	0.444
0.001	2.283	0.438
0.01	2.344	0.427
0.1	2.319	0.431
1	2.287	0.437
10	2.293	0.436
100	2.317	0.432
1 000	2.241	0.446
10 000	2.230	0.448

into the cell in-contact with the gold layer. Figure 6 shows the SPR reflectivity curves for the gold layer interact with DW. From the curve, the resonance angle obtained was 53.93°. The experiment was then conducted using AA with varying concentrations ranging from 0 to 10,000 μM. A series of injections of AA at various concentrations were made into the hollow cell linked to the gold layer. Figure 7 displays the SPR reflectivity curves of AA in-contact with the gold thin film. Based on Fig. 8, all concentrations of AA were found to have a resonance angle of 53.93°, which was identical to the resonance angle of deionized water. It is verified that the gold thin film's resonance angle value toward different AA concentrations remains unchanged. This outcome could be explained by the fact that just a tiny amount of AA was absorbed into the sensing layer and bring no changes in the value of resonance angle.

The experiment was continued by substituting the gold thin film with the Au/CQD thin film. SPR reflectivity curves were plotted for AA concentrations ranging from 0 to 10,000 μM, as shown in Fig. 9. Based on the figure, there was a noticeable shift in the resonance angle toward higher values as AA concentration increased. This shift can be attributed to the interaction between AA and the Au/CQD thin film, which raised the refractive index of the sensing layer, resulting in a more substantial change in the resonance angle. Additionally, the increase in molecule binding to the thin film likely contributed to this shift in the resonance angle [73, 74].

To determine the sensitivity of the Au/CQDs-based sensor, the shift in resonance angle ($\Delta\theta$) was plotted against the concentration of AA. The $\Delta\theta$ values were calculated by measuring the difference in resonance angle between each AA concentration and DW as a reference. Table 1 presents the resonance angles and corresponding shifts for AA concentrations ranging from 0 to 10,000 μM, with CQDs deposited on the gold layer. Figure 10 illustrates that the presence of CQDs on the gold layer enhances the SPR sensor's sensitivity for AA detection, as evidenced by an increase in resonance angle with rising AA concentration up to 10,000 μM. The linear fit of resonance angle shift versus AA concentration shows a strong response, with a linear regression coefficient (R^2) of 0.961. The slope of 0.026° μM^{-1} for AA concentrations between 0 and 10 mM confirms that the sensitivity of the sensor is improved with the addition of CQDs. The limit of detection (LoD) was also calculated using the standard formula of

$$LoD = \frac{3\sigma}{S} \tag{1}$$

where σ is the standard deviation of resonance angle at 0 μM, and S is the sensitivity. Based on repeated measurements, the standard deviation was 0.01°, resulting in LoD of approximately 1.15 μM. This result shows the critical role of CQDs for sensing AA with lowest detection of 0.001 μM in the range of 0.001 to 10,000 μM and LoD of approximately 1.15 μM. The performance of the proposed sensor for AA detection was evaluated against other reported sensors based on different materials, with the comparative results summarized in Table 2.

The full width at half maximum (FWHM) and detection accuracy (DA) were also calculated to further investigate the performance of the sensor. The FWHM can be determined by measuring the width of the SPR reflectivity curve corresponding to the half value of the maximum reflectance as shown in Fig. 11. The DA was calculated as the inverse of FWHM. The SPR reflectivity curve's width determines the DA of the sensor. The narrower the SPR reflectivity curve, the higher the DA [86]. All the measured data of the FWHM and DA of the Au/CQD-based sensor upon adsorption of AA are shown in Table 3.

From the table, it can be concluded that no significant patterns have been noticed for the FWHM and the DA where

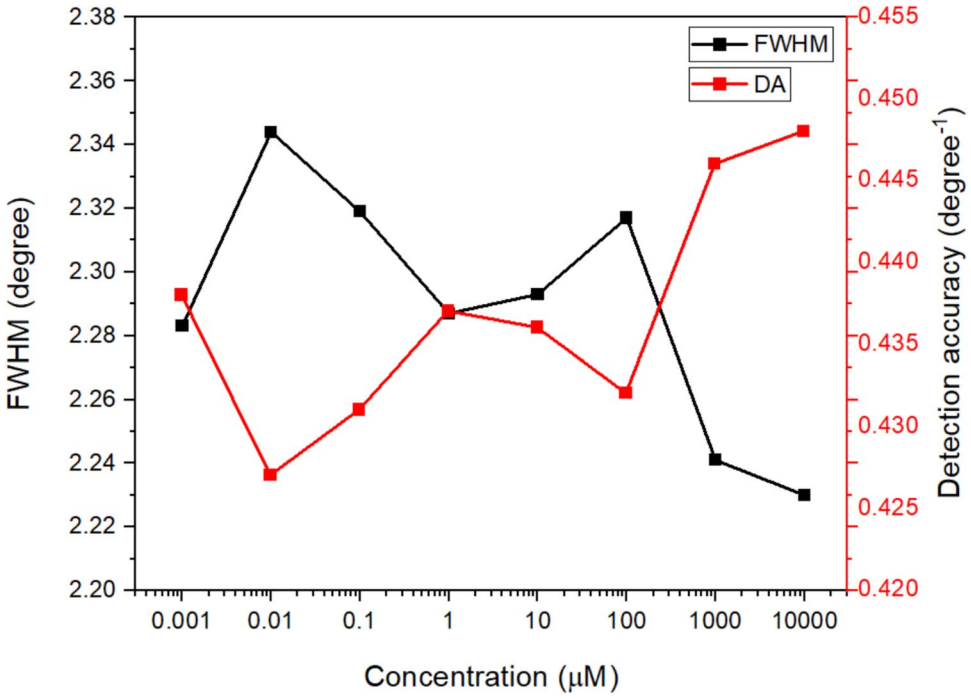

Fig. 12 FWHM and DA of the Au/CQD SPR sensor towards AA

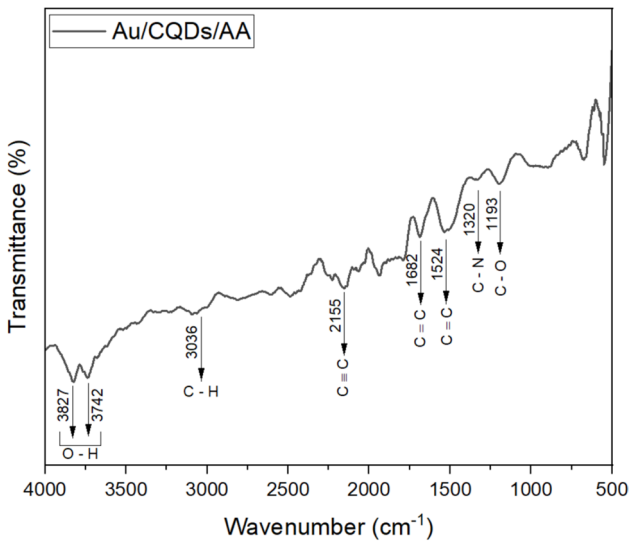

Fig. 13 FTIR spectrum of Au/CQD thin film after being in-contact with AA

most of the values are in the range of 2.230° to 2.344° and 0.427/° to 0.448/° for the FWHM and DA respectively. The plot for FWHM and DA of this SPR sensor towards AA is shown in Fig. 12. The widths of the SPR reflectivity curves were nearly identical, and the only parameter that differs was the position of the resonance angle, indicating that varying AA concentrations have little to no impact on the DA of this sensor.

To investigate the interaction between AA and the CQD thin film, FTIR characterization was conducted following their exposure. The resulting FTIR spectrum for the Au/CQD thin film, now in contact with AA, showed increased intensity in specific functional groups. As seen in Fig. 13, the intensity of two characteristic O–H peaks increased after AA was introduced to the thin film. Similarly, the peaks at 1682 cm^{-1} and 1524 cm^{-1}, corresponding to C = C bonds, also exhibited heightened intensity. These observed changes confirm the presence of AA within the CQD thin film after exposure. The changes of this functional groups also suggest that AA may interact with CQDs through hydrogen bonding that lead to the increase in sensitivity of the SPR sensor [87].

Additionally, the structural properties of the Au/CQDs thin film after interacting with AA were investigated using AFM. As shown in Fig. 14, AA absorption on the sensor surface led to noticeable changes in surface morphology. While the general peak structure of the CQDs remained similar before and after AA exposure, the RMS roughness increased from 0.736 to 0.975 nm following AA injection. This increase in roughness aligns with previous findings, indicating that CQDs exhibit higher RMS roughness after interactions with other materials [88]. The altered surface morphology upon AA binding demonstrates a more heterogeneous film, which can enhance the SPR signal's sensitivity by amplifying the film's interaction with the analyte. This morphological change highlights the role of surface roughness in optimizing SPR sensor performance, providing a crucial parameter for achieving high sensitivity in AA detection.

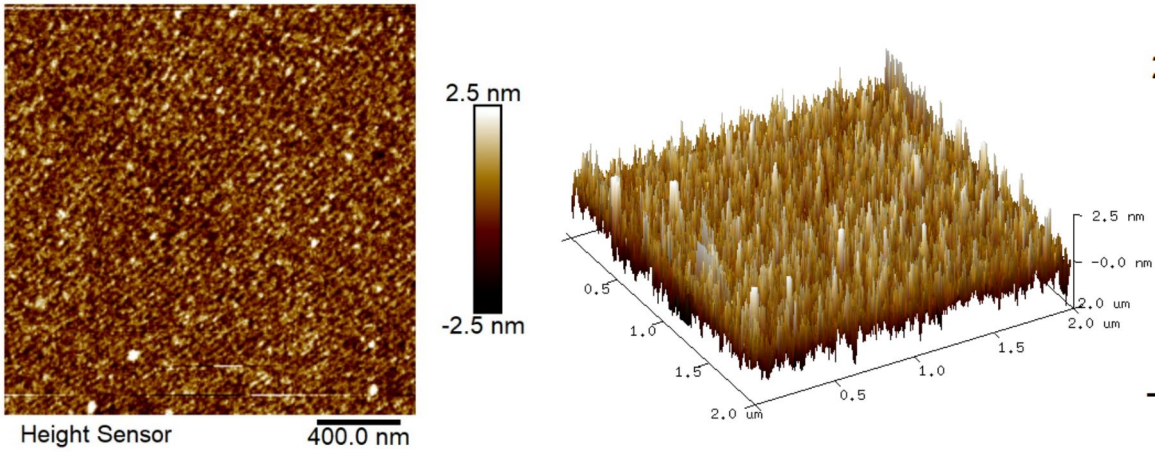

Fig. 14 AFM result of the Au/QD thin film after interaction with AA

Conclusion

In this research, the structural and optical properties of Au/CQDs thin film for potential sensing of ascorbic acid (AA) using SPR have been successfully demonstrated. The FTIR result confirmed the presence of O–H, C–H, C≡C, C–N, and C–O on the surface of the thin film. The AFM images revealed that the thin film has a uniform spiky surface with RMS roughness of 0.736 nm. For the optical properties, the Au/CQD thin film has an absorbance peak of approximately 4.44 in the range of 260 to 270 nm with optical band gap of 4.072 eV. Furthermore, the Au/CQD thin film showed a good potential for AA detection. Integration of Au/CQD thin film with SPR resulted in significant shifts in the SPR reflectivity curve with increasing concentrations of AA, revealing a high sensitivity of 0.026° μM^{-1} across a wide concentration range from 0.001 to 10,000 µM. Moreover, the calculated FWHM and DA of the sensor are in the range of 2.230° to 2.344° and 0.427/° to 0.448/° respectively. When investigated using FTIR, exposure of AA on the Au/CQD thin film caused changes in the oxygen-containing functional groups present on the thin film surface. This interaction then leads to the enhanced sensitivity of the sensor. AFM imaging further validated the interaction, showing an increase in RMS roughness from 0.736 to 0.975 nm upon AA binding, supporting that AA adsorption notably impacts the film's morphology and enhances SPR sensor responsiveness. The consistent interaction between AA and the Au/CQD thin film demonstrates the sensor's potential for highly sensitive AA detection.

Acknowledgements The laboratory facilities provided by the Faculty of Science, Institute of Nanoscience and Nanotechnology, and Faculty of Engineering, Universiti Putra Malaysia, are acknowledged.

Author Contribution Research and investigation, W.M.E.M.M.D.; formal analysis, W.M.E.M.M.D. and M.Z.K.; writing original draft preparation, W.M.E.M.M.D. and M.Z.K.; writing—review and editing, W.M.E.M.M.D., M.Z.K., N. I.M.F., H.S.H., M.F.A., F.B.K.E., and Y.W.F.; conceptualization, Y.W.F., F.A.A.N., N.H., H.A., and A.T.,; supervision, Y.W.F.; funding acquisition, Y.W.F.;. All authors have read and agreed to the published version of the manuscript.

Funding Open access funding provided by The Ministry of Higher Education Malaysia and Universiti Putra Malaysia. This research was funded by Universiti Putra Malaysia through Putra Grant (GPB/2024/9810900).

Data Availability No datasets were generated or analysed during the current study.

Declarations

Competing interests The authors declare no competing interests.

References

1. Iron C, Sabatier M, Rytz A, Husny J (2020) Impact of ascorbic acid on the in vitro iron bioavailability of a casein-based iron fortifica. Nutrients 12:2776
2. Savan EK, Ozcan I, Koytepe S (2022) Preparation of mesoporous carbon containing Polyurethane/Clay nanocomposite membrane based sensors for sensitive and selective determination of vitamin D 2 in urine samples. Measurement 203:111979
3. Naidu KA (2003) Vitamin C in human health and disease is still a mystery ? An overview. Nutr J 10:1–10
4. Prakash S, Chakrabarty T, Rajesh AM, Shahi VK (2012) Investigation of polyelectrolyte for electrochemical detection of uric acid in presence of ascorbic acid. Measurement 45:500–506
5. Ravetti S, Clemente C, Hergert L et al (2019) Ascorbic acid in skin health. Cosmetics 6:6–13
6. Moon KM, Kwon E, Lee B, Kim CY (2020) Recent trends in controlling the enzymatic browning of fruit and vegetable products. Molecules 25:2574
7. Panel E, Nda A (2013) Scientific opinion on dietary reference values for vitamin C1. Eur Food Saf Auth 11:1–68
8. Carr AC, Rosengrave PC, Bayer S et al (2017) Hypovitaminosis C and vitamin C deficiency in critically ill patients despite recommended enteral and parenteral intakes. Crit Care 300:1–10
9. Zare HR, Moradiyan B, Shekari Z, Benvidi A (2016) Application of L-DOPA modified carbon nanotubes as a bifunctional electrocatalyst for simultaneous determination of ascorbic acid, adrenaline, acetaminophen and tyrosine. Measurement 90:510–518
10. Hatefi-mehrjardi A, Ali M, Soleymanzadeh M, Barani A (2020) Highly sensitive detection of dopamine, ascorbic and uric acid with a nanostructure of dianix yellow / multi-walled carbon nanotubes modified electrode. Measurement 163:107893
11. Shrivastav AM, Usha SP, Gupta BD (2016) Fiber optic profenofos sensor based on surface plasmon resonance technique and molecular imprinting. Biosens Bioelectron 79:150–157
12. Mansouri M, Fathi F, Jalili R et al (2020) SPR enhanced DNA biosensor for sensitive detection of donkey meat adulteration. Food Chem 331:127163–127172
13. Xue T, Liang W, Li Y et al (2019) Ultrasensitive detection of miRNA with an antimonene-based surface plasmon resonance sensor. Nat Commun 10:1–9
14. Yang HM, Teoh JY, Yim GH et al (2020) Label-free analysis of multivalent protein binding using bioresponsive nanogels and surface plasmon resonance (SPR). ACS Appl Mater Interfaces 12:5413–5419
15. Yao GH, Liang RP, Huang CF et al (2013) Surface plasmon resonance sensor based on magnetic molecularly imprinted polymers amplification for pesticide recognition. Anal Chem 85:11944–11951
16. Ansari G, Kanjariya P, Reddy MS et al (2025) Refractive index sensing-based surface plasmon resonance sensor for sensitivity enhancement: theoretical analysis. Plasmonics. https://doi.org/10.1007/s11468-025-03082-5
17. Ansari G, Oweis R, Baldaniya L et al (2025) Early detection of chikungunya virus using silver and zinc selenide multilayer structure utilizing the surface plasmon resonance: a numerical approach. Plasmonics. https://doi.org/10.1007/s11468-025-02978-6
18. Yang X, Singh H, Uniyal A et al (2025) Surface plasmon resonance-based cortisol sensing: a numerical investigation. Plasmonics, https://doi.org/10.1007/s11468-025-02895-8
19. Howe CL, Webb KF, Abayzeed SA et al (2019) Surface plasmon resonance imaging of excitable cells. J Phys D Appl Phys 52:104001
20. Zhang S, Li J, Li S et al (2018) Surface plasmon resonance sensor based on D-shaped photonic crystal fiber with two micro-openings. J Phys D Appl Phys 51:305104
21. Uniyal A, Kumar M, Kumar R, Dhiman G (2025) Silver, silicon, and selenium-based surface plasmon resonance sensor for pathogen bacteria detection in visible region. Opt Quantum Electron 57:196
22. Fen YW, Yunus WMM, Talib ZA (2013) Analysis of Pb(II) ion sensing by crosslinked chitosan thin film using surface plasmon resonance spectroscopy. Optik (Stuttg) 124:126–133
23. Chah S, Yi J, Zare RN (2004) Surface plasmon resonance analysis of aqueous mercuric ions. Sensors Actuators, B Chem 99:216–222
24. Yu JCC, Lai EPC, Sadeghi S (2004) Surface plasmon resonance sensor for Hg(II) detection by binding interactions with polypyrrole and 2-mercaptobenzothiazole. Sensors Actuators, B Chem 101:236–241
25. Sadrolhosseini AR, Noor ASM, Bahrami A et al (2014) Application of polypyrrole multi-walled carbon nanotube composite layer for detection of mercury, lead and iron ions using surface plasmon resonance technique. PLoS ONE 9:e93962–e93971
26. Lee SM, Kang SW, Kim DU et al (2001) Effect of metal ions on the absorption spectra and surface plasmon resonance of an azacrown indoaniline dye. Dye Pigment 49:109–115
27. Hur Y, Ock K, Kim K et al (2002) Surface plasmon resonance study on enhanced refractive index change of an Ag^{+} ion-sensing membrane containing dithiosquarylium dye. Anal Chim Acta 460:133–139
28. Pelossof G, Tel-Vered R, Willner I (2012) Amplified surface plasmon resonance and electrochemical detection of Pb^{2+} ions using the Pb^{2+}-dependent DNAzyme and hemin/G-quadruplex as a label. Anal Chem 84:3703–3709
29. Saleviter S, Fen YW, Alia N et al (2017) Development of optical sensor for determination of Co (II) based on surface plasmon resonance phenomenon. Sens Lett 15:1–6
30. Zaman MU, Ansari G, Uniyal A et al (2025) Antimonene, barium titanate and silver layer–based surface plasmon resonance sensor for dental application: a numerical analysis. Plasmonics. https://doi.org/10.1007/s11468-025-03020-5
31. Ock K, Jang G, Roh Y et al (2001) Optical detection of Cu^{2+} ion using a SQ-dye containing polymeric thin-film on Au surface. Microchem J 70:301–305
32. Daniyal WMEMM, Fen YW, Abdullah J et al (2018) Exploration of surface plasmon resonance for sensing copper ion based on nanocrystalline cellulose-modified thin film. Opt Express 26:34880–34893
33. Ramdzan NSM, Fen YW, Omar NAS et al (2019) Optical and surface plasmon resonance sensing properties for chitosan/carboxyl-functionalized graphene quantum dots thin film. Optik (Stuttg) 178:802–812
34. Forzani ES, Zhang H, Chen W, Tao N (2005) Detection of heavy metal ions in drinking water using a high-resolution differential surface plasmon resonance sensor. Environ Sci Technol 39:1257–1262
35. Chen H, Gal Y-S, Kim S-H et al (2008) Potassium ion sensing using a self-assembled calix[4]crown monolayer by surface plasmon resonance. Sensors Actuators B Chem 133:577–581
36. Fahnestock KJ, Manesse M, McIlwee HA et al (2009) Selective detection of hexachromium ions by localized surface plasmon resonance measurements using gold nanoparticles/chitosan composite interfaces. Analyst 134:881–886
37. Chang CC, Lin S, Wei SC et al (2011) An amplified surface plasmon resonance "turn-on" sensor for mercury ion using gold nanoparticles. Biosens Bioelectron 30:235–240

38. May LM, Russell DA (2003) Novel determination of cadmium ions using an enzyme self-assembled monolayer with surface plasmon resonance. Anal Chim Acta 500:119–125
39. Wu CM, Lin LY (2005) Utilization of albumin-based sensor chips for the detection of metal content and characterization of metal-protein interaction by surface plasmon resonance. Sensors Actuators, B Chem 110:231–238
40. Al-rekabi SH, Kamil YM, Bakar MHA et al (2019) Hydrous ferric oxide-magnetite-reduced graphene oxide nanocomposite for optical detection of arsenic using surface plasmon resonance. Opt Laser Technol 111:417–423
41. Saleviter S, Fen YW, Omar NAS et al (2018) Optical and structural characterization of immobilized 4-(2-pyridylazo) resorcinol in chitosan-graphene oxide composite thin film and its potential for Co^{2+} sensing using surface plasmon resonance technique. Results Phys 11:118–122
42. Wang L, Li T, Du Y et al (2010) Au NPs-enhanced surface plasmon resonance for sensitive detection of mercury(II) ions. Biosens Bioelectron 25:2622–2626
43. Speranza G (2021) Carbon nanomaterials: synthesis, functionalization and sensing applications. Nanomaterials 11:967
44. Gupta BD, Pathak A, Semwal V (2019) Carbon-based nanomaterials for plasmonic sensors: a review. Sensors 19:3536
45. Scida K, Stege PW, Haby G et al (2011) Recent applications of carbon-based nanomaterials in analytical chemistry : Critical review. Anal Chim Acta 691:6–17
46. Zhang B, Zheng X, Li H, Lin J (2013) Application of carbon-based nanomaterials in sample preparation : a review. Anal Chim Acta 784:1–17
47. Li M, Chen T, Gooding JJ, Liu J (2019) Review of carbon and graphene quantum dots for sensing. ACS Sensors 4:1732–1748
48. Devi P, Rajput P, Thakur A, Kim K (2019) Recent advances in carbon quantum dot-based sensing of heavy metals in water. Trends Anal Chem 114:171–195
49. Tian L, Li Z, Wang P et al (2021) Carbon quantum dots for advanced electrocatalysis. J Energy Chem 55:279–294
50. Rao N, Singh R, Bashambu L (2021) Carbon-based nanomaterials : synthesis and prospective applications. Mater Today Proc 44:608–614
51. Yin F, Yue W, Li Y et al (2021) Carbon-based nanomaterials for the detection of volatile organic compounds : a review. Carbon N Y 180:274–297
52. Xie F, Yang M, Jiang M et al (2019) Carbon-based nanomaterials-a promising electrochemical sensor toward persistent toxic substance. Trends Anal Chem 119:115624
53. Eddin FBK, Fen YW, Omar NAS et al (2021) Femtomolar detection of dopamine using surface plasmon resonance sensor based on chitosan/graphene quantum dots thin film. Spectrochim Acta - Part A Mol Biomol Spectrosc 263:120202
54. Amini N, Shamsipur M, Bagher M, Barati A (2017) A glassy carbon electrode modified with carbon quantum dots and polyalizarin yellow R dyes for enhanced electrocatalytic oxidation and nanomolar detection of L-cysteine. Microchem J 131:9–14
55. Muthusankar G, Sangili A, Chen S et al (2018) In situ assembly of sulfur-doped carbon quantum dots surrounded iron (III) oxide nanocomposite; a novel electrocatalyst for highly sensitive detection of antipsychotic drug olanzapine. J Mol Liq 268:471–480
56. Shereema RM, Rao TP, Kumar VBS et al (2018) Individual and simultaneous electrochemical determination of metanil yellow and curcumin on carbon quantum dots based glassy carbon electrode. Mater Sci Eng C 93:21–27
57. Khan ME, Mohammad A, Yoon T (2022) State-of-the-art developments in carbon quantum dots (CQDs): photo-catalysis, bioimaging, and bio-sensing applications. Chemosphere 302:134815
58. Loo AH, Sofer Z, Bous D et al (2016) Carboxylic carbon quantum dots as a fluorescent sensing platform for DNA detection. Appl Mater Interfaces 8:1951–1957
59. Afifah N, Nazri A, Hidayah N et al (2021) Carbon quantum dots for optical sensor applications : a review. Opt Laser Technol 139:106928
60. Kumar S, Yang D, Koppala S et al (2019) Highly photoluminescent N, P doped carbon quantum dots as a fluorescent sensor for the detection of dopamine and temperature. J Photochem Photobiol B Biol 194:61–70
61. Ahn H, Song H, Choi JR, Kim K (2018) A localized surface plasmon resonance sensor using double-metal-complex nanostructures and a review of recent approaches. Sensors 18:98
62. Tangkawsakul W, Srikhirin T, Shinbo K et al (2016) Application of long-range surface plasmon resonance for ABO blood typing. Int J Anal Chem 2016:1432781
63. Sharma V, Dwivedi LK, Singh S et al (2025) Analytical study on effect of perovskite halides based surface plasmon resonance sensor for detection of sugar content in soft drinks. Sens Imaging 26:1–19
64. Uniyal A, Kumba K, Dhiman G et al (2024) Advanced SPR sensor for human sperm analysis: leveraging silver and nanomaterials for enhanced performance. Plasmonics 20:3939–3950
65. Uniyal A, Ansari G, Kumba K et al (2025) 17-An optimized design of SPR sensor with TiSi2/MXene/CNT multilayer structures: a TMM reflectance study using angle interrogation for haemoglobin detection. Metaheuristics-Based Materials Optimization 2025: 433–454
66. Eddin FBK, Fen YW, Fauzi NIM et al (2022) Direct and sensitive detection of dopamine using carbon quantum dots based refractive index surface plasmon resonance sensor. Nanomaterials 12:1799
67. Wang X, Yang P, Feng Q et al (2019) Green preparation of fluorescent carbon quantum dots from cyanobacteria for biological imaging. Polymers (Basel) 11:616
68. Liu S, Na W, Pang S, Su X (2014) Fluorescence detection of Pb^{2+} based on the DNA sequence functionalized CdS quantum dots. Biosens Bioelectron 58:17–21
69. He M, Zhang J, Wang H et al (2018) Material and optical properties of fluorescent carbon quantum dots fabricated from lemon juice via hydrothermal reaction. Nanoscale Res Lett 13:175
70. Omar NAS, Fen YW, Abdullah J et al (2020) Sensitive detection of dengue virus type 2 E-proteins signals using self-assembled monolayers/reduced graphene oxide-PAMAM dendrimer thin film-SPR optical sensor. Sci Rep 10:1–15
71. Ding Y, Zhang F, Xu J et al (2017) Synthesis of short-chain passivated carbon quantum dots as the light emitting layer towards electroluminescence. RSC Adv 7:28754–28762
72. Ramdzan NSM, Fen YW, Liew JYC et al (2021) Exploration on structural and optical properties of nanocrystalline cellulose/poly(3,4-ethylenedioxythiophene) thin film for potential plasmonic sensing application. Photonics 8:419
73. Nasuha S, Yatim N, Rozana A et al (2023) Visible and angular interrogation of Kretschmann-based SPR using hybrid Au – ZnO optical sensor for hyperuricemia detection. Heliyon 9:e22926
74. Fahmy H, Salah A, Fattah GA (2022) Determination of refractive indices of heavy metal ions solutions to evaluate their concentrations. Egypt J Chem 65:321–330
75. Peng J, Ling J, Zhang X et al (2015) A rapid, sensitive and selective colorimetric method for detection of ascorbic acid. Sensors Actuators B Chem 221:708–716
76. Sumra S, Humera N, Asma A et al (2022) Sensitive and highly selective colorimetric biosensing of vitamin-C and vitamin-B1 by flavoring agent - based silver nanoparticles. JBIC J Biol Inorg Chem 27:471–483

77. Wang H, Lv P, Liu C et al (2022) Cerium-based nanoparticles triggered catalytic reaction for the colorimetric and ratiometric fluorimetric dual-signal sensing of vitamin C. Spectrochim Acta Part A Mol Biomol Spectrosc 278:121324
78. Gong X, Liu Y, Yang Z et al (2017) Analytica Chimica Acta An "on-off-on" fl uorescent nanoprobe for recognition of chromium (VI) and ascorbic acid based on phosphorus / nitrogen dual- doped carbon quantum dot. Anal Chim Acta 968:85–96
79. Liu J, Chen Y, Wang W et al (2016) "Switch-on" fluorescent sensing of ascorbic acid in food samples based on carbon quantum dots−MnO 2 probe. Africultural Food Chem 64:371–380
80. Msto RK, Othman HO, Al-hashimi BR et al (2023) Fluorescence turns on-off-on sensing of ferric ion and L-ascorbic acid by carbon quantum dots. Journal Food Qual 2023:5555608
81. Li L, Wang C, Luo J et al (2015) Fe^{3+}-functionalized carbon quantum dots : a facile preparation strategy and detection for ascorbic acid in rat brain microdialysates. Talanta 144:1301–1307
82. Preethi M, Murugan R, Viswanathan C, Ponpandian N (2022) Potato starch derived N-doped carbon quantum dots as a fluorescent sensing tool for ascorbic acid. J Photochem Photobiol A Chem 431:114009
83. Huang L, Qin S, Yang K et al (2024) Dual signal AA detection based on fluorescence and local surface plasmon resonance absorption technology. Spectrochim Acta Part A Mol Biomol Spectrosc 306:123570
84. Kumar S, Member S, Singh R et al (2021) Highly sensitive, selective and portable sensor probe using germanium-doped photosensitive optical fiber for ascorbic acid detection. IEEE Sens J 21:62–70
85. Zarei K, Moghaddary S (2015) Sensitive spectrophotometric determination of ascorbic acid in drugs and foods using surface plasmon resonance band of silver nanoparticles sensitive spectrophotometric determination of ascorbic acid in drugs and foods using surface plasmon resonance band. Cogent Chem 1:1109172
86. Kamaruddin N, Bakar AA, Mobarak N et al (2017) Binding affinity of a highly sensitive Au/Ag/Au/chitosan-graphene oxide sensor based on direct detection of Pb^{2+} and Hg^{2+} ions. Sensors 17:2277–2287
87. Ayad MM, Abdelghafar ME, Torad NL et al (2023) Green synthesis of carbon quantum dots toward highly sensitive detection of formaldehyde vapors using QCM sensor. Chemosphere 312:137031
88. Chen X, Yan R, Zhang W, Fan J (2016) Carrier recombination spatial transfer by reduced potential barrier causes blue/red switchable luminescence in C8 carbon quantum dots/organic hybrid light-emitting devices. APL Mater 4:046102